Challenge Journal of Structural Mechanics

Research Article

Investigating the effects of glass fiber in enhancing concrete pavement performance

Fatih İrfan Baş [a,*]

[a] *Department of Civil Engineering, Erzincan Binali Yıldırım University, 24002 Erzincan, Türkiye*

ABSTRACT

Flexible pavements are considered more sustainable than concrete pavements primarily due to the higher long-term maintenance and rehabilitation costs associated with concrete pavements. Concrete pavements possess a higher modulus of elasticity, which allows them to distribute vehicle loads over a larger area, thereby enhancing the strength of the pavement. However, despite this advantage, their flexural strength is relatively low. As a result, there has been a growing focus on research to improve the flexural strength of concrete pavements to increase their overall performance and sustainability. This study aimed to reveal the effects of enhanced mechanical properties of concrete reinforced with glass fiber on concrete pavements, specifically under heavy vehicle loading as in real-world conditions. The impact of glass fiber on the thickness of both the concrete and base layers, as well as the quality of the base layer material and transverse joint spacing, was assessed. For this purpose, 3D finite element models were developed using ANSYS software, considering concrete thicknesses of 100, 150, and 200 mm, glass fiber ratios of 0%, 0.5%, and 1%, base layer elastic moduli of 100, 200, and 300 MPa, and transverse joint spacings of 300, 450, and 600 mm. It was determined that the concrete thickness and the base layer modulus of elasticity were the most influential factors in minimizing flexural stress, total deformation, and equivalent total strain. The glass fiber addition had a more notable impact on maximum principal stress, especially at the 1% ratio, but had a minimal effect on total deformation and strain. Transverse joint spacing had the least effect, although shorter spacings are still recommended to reduce the risk of transverse cracking in stiffer base layers.

ARTICLE INFO

Article history:
Received – November 18, 2024
Revision requested – December 16, 2024
Revision received – December 23, 2024
Accepted – January 4, 2025

Keywords:
glass fiber
concrete pavement
cast iron model
Taguchi method
finite element model

Citation: Baş Fİ (2025). Investigating the effects of glass fiber in enhancing concrete pavement performance. *Challenge Journal of Structural Mechanics*, 11(1), 42–54.

1. Introduction

Flexible pavements have a lower initial cost; however, when long-term maintenance costs are considered, they are more expensive than concrete pavements (Nazki et al. 2020; Araz et al. 2023). In Türkiye, 92% of the 2024 transportation maintenance budget is allocated primarily for flexible pavements (KGM 2024). Therefore, expanding the use of concrete pavement applications in both Türkiye and globally is essential at the earliest opportunity. Concrete pavements have a higher elasticity modulus and stiffness than flexible pavements, enabling them to spread traffic loads over a wider area on the ground, which enhances their strength. They function similarly to beams resting on an elastic foundation (Ağar et al. 1998). Plain concrete, however, is a brittle material, and its flexural strength decreases as its strength class increases (Zain et al. 2002). Flexural strength measures a material's resistance to bending stresses, indicating the stress level at which it fails in bending (Ntimugura et al. 2020). For concrete, flexural strength typically ranges from 10% to 20% of its compressive strength (Kosmatka et al. 2003).

* *Corresponding author*. Tel.: +90-446-224-0088 ; E-mail address: fibas@erzincan.edu.tr (F. İ. Baş)
ISSN: 2149-8024 / DOI: https://doi.org/10.20528/cjsmec.2025.01.004

Studies aimed at enhancing flexural strength have led to a rapid increase in the use of various additives and fibers (steel, basalt, glass, polymeric, carbon) in plain concrete, as reflected in the literature (Çelik et al. 2024). The utilization of fibers improves the service life and mechanical properties of concrete (Karahan and Atiş 2011; Zhang and Li 2013; Şengel et al. 2022; Gultekin 2023; Eryılmaz Yıldırım et al. 2024). Glass fibers are the most commonly used synthetic fibers to enhance the flexural strength of concrete, a critical parameter for concrete pavements under cyclic loading, owing to their availability and ease of application (Akram et al. 2024).

Jagannadha and Ahmed (2009) revealed that incorporating just 0.03% glass fiber into plain concrete resulted in greater flexural and compressive strengths compared to both 0.1% glass fiber and plain concrete. Kizilkanat et al. (2015) conducted a study using glass fiber and basalt fiber and reported that splitting tensile strength improved with increasing basalt fiber ratios; however, no further increase was observed beyond a 0.5% glass fiber ratio. Afroz et al. (2019) demonstrated that a 1% addition of steel fiber increased flexural and compressive strengths by 80% and 10%, respectively. Ali and Qureshi (2019) observed that adding 0.25% to 1.0% glass fiber to concrete enhanced its flexural strength by 25%. Lau et al. (2020) found that fiber addition increased fatigue cycles in concrete pavements by 135%. Hussain et al. (2020) concluded that a 1% addition of steel fiber reduced pavement thickness by 34%. Tunçel et al. (2020) reported that 0.5% Kevlar fiber improved the flexural strength of concrete pavements. Abdulridha et al. (2021) investigated the effects of varying cement content, steel and polypropylene fiber ratios, and silica fume ratios, concluding that cement content had the greatest impact on reducing shrinkage cracking. Sharbatdar and Rahmati (2022) reported that adding 20 kg of steel fibers per m^3 increased flexural and tensile strengths by 83% and 20%, respectively. Bhogone and Subramaniam (2022) observed that hybrid use of polypropylene and steel fibers reduced plastic shrinkage cracking by 90%. Mola et al. (2024) studied Kevlar fiber's effect on concrete pavements, finding that it enhanced flexural and compressive strengths by 15% and 5%, respectively.

In recent years, there has been a growing focus on the numerical modeling of fiber-reinforced concrete. The finite element method offers a numerical approach for addressing issues involving complex structures, varying loads, and diverse materials.

Kumara et al. (2003) developed a finite element model to examine flexural stresses in ultra-thin pavements, observing that Florida pavement test sections in poor condition generated higher flexural stresses beneath the concrete layer. Sultana (2010) developed a finite element model using SolidWorks software to analyze the bonding conditions between whitetopping concrete and flexible pavements. The findings indicated that bond conditions were the most critical factor influencing pavement performance, with increased concrete layer thickness resulting in reduced flexural stress beneath the concrete layer. Çelik (2014) reported that, in a finite element model subjected to tandem axle dual tire loading, flexible pavements exhibited vertical stress levels 119% higher than those in concrete pavements. Additionally, Baş et al. (2022) developed a 3D finite element model to investigate flexural stresses in concrete pavements constructed on deteriorated flexible bases, concluding that concrete thickness was the most influential parameter in controlling bending stresses under the concrete layer.

In addition to the purchase costs of fibers used to enhance flexural strength, their impact on reducing workability, requiring the use of plasticizers, adds significant costs to the overall pavement design. Therefore, to make the use of fiber in concrete pavements more feasible, it is essential to reduce the thickness of the concrete layer, as well as the thickness and rigidity (quality) of the base layer. Besides, standard beam flexural strength tests often cannot be reliably used to estimate concrete pavement performance (Roesler et al. 2004).

This study aimed to investigate the effects of enhanced mechanical properties of concrete reinforced with glass fiber on the performance of concrete pavements under heavy vehicle loading, reflecting real-world conditions. The influence of glass fiber on the thickness of both the concrete and base layers, as well as the quality of the base layer material, was evaluated. Nonlinear finite element analysis was performed using ANSYS (SAS 2024) software with a cast iron material model. Finite element models were developed based on the Taguchi experimental design method, incorporating parameters such as concrete thicknesses of 100, 150, and 200 mm, glass fiber ratios of 0%, 0.5%, and 1%, base layer elastic moduli of 100, 200, and 300 MPa, and transverse joint spacings of 300, 450, and 600 mm.

2. Materials and Method

When complex problems cannot be solved directly, the main problem can be divided into smaller and more manageable sub-problems called finite elements. The solution to the original problem can then be obtained from the solutions to these sub-problems. In this process, a sufficient model can be obtained using a well-defined finite number of elements (Moaveni 2011). Cheung and Zinkiewicz (1965) were the first to apply finite element analysis for pavement analysis.

2.1. Finite element modeling

Ali et al. (2020) conducted an in-depth study on the effects of adding glass fiber to pavement concrete, examining its mechanical properties at fiber ratios of 0%, 0.5%, and 1%. They evaluated compressive strength and elastic modulus in accordance with ASTM-C39 (2015). Additionally, flexural strength was assessed using a four-point loading test on 100 x 100 x 350 mm specimens, following ASTM-C78 (2018). In this study, the findings of Ali et al. (2020) were applied to evaluate the effects of glass fiber on concrete pavement via finite element modeling. The load-deflection curve from the bending test is shown in Fig. 1, and Table 1 summarizes the mechanical properties of both plain and glass fiber reinforced concrete.

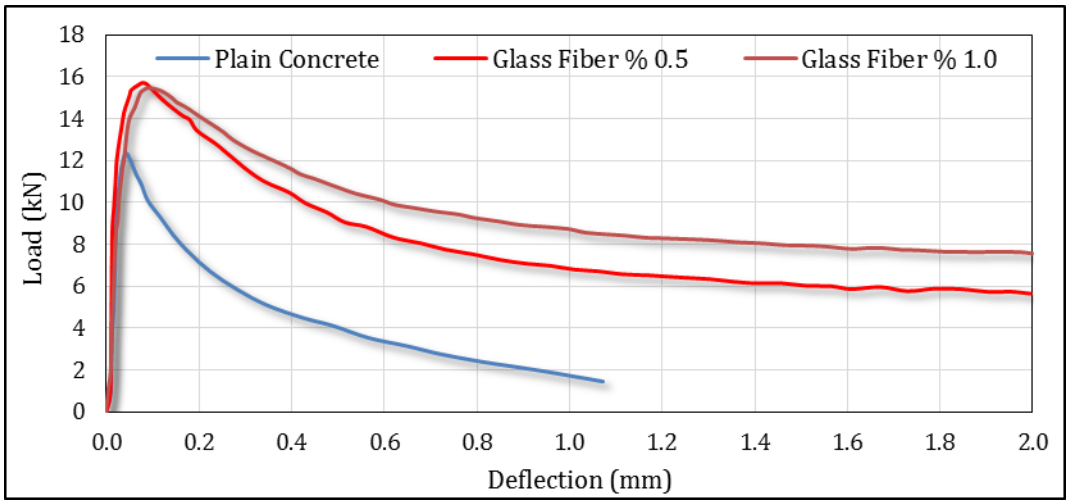

Fig. 1. Load deflection data of plain concrete and glass fiber reinforced concretes.

Table 1. Mechanical properties of plain and glass fiber reinforced concretes.

Type	Compressive strength (MPa)	Elastic modulus (MPa)	Flexural strength (MPa)
Plain concrete	34.66	23472	3.79
Glass fiber % 0.5	36.87	24583	4.75
Glass fiber % 1.0	35.57	23842	4.68

The Cast Iron plasticity model was utilized to capture the non-linear behavior of glass fiber-reinforced concrete, incorporating compressive and tensile stress-strain test data (Nguyen Dinh 2016; Jawdhari and Fam 2020; Noorvand et al. 2022). As the load-deflection data for compression tests were not provided in the study and only compression yield strengths were available, load-deflection curves were generated based on these yield strengths. This model presumes identical elastic behavior in both tension and compression; therefore, the division of stress by strain in the initial rows of compression and flexural tests was idealized to be the same, ensuring consistent results. Table 2 summarizes the stress–strain input values for the flexural response used in the Cast Iron plasticity model for both plain and glass fiber-reinforced concretes, based on experimental data.

Table 2. Flexural response input parameters for finite element analysis.

Plain concrete		Glass fiber % 0.5		Glass fiber % 1.0	
Strain (mm/mm)	Stress (MPa)	Strain (mm/mm)	Stress (MPa)	Strain (mm/mm)	Stress (MPa)
0.00010	2.35	0.00010	2.46	0.00005	1.19
0.00024	3.03	0.00024	3.64	0.00021	2.48
0.00043	3.79	0.00034	4.09	0.00029	3.08
		0.00039	4.29	0.00036	3.49
		0.00055	4.60	0.00046	4.04
		0.00085	4.75	0.00072	4.53
				0.00078	4.60
				0.00094	4.68

Axle weight studies conducted on 14,488 vehicles across 79 locations in Türkiye show that the most common truck type, representing 32% of the sample, has a 1.22 axle configuration (KGM 2023). For finite element analysis, heavy vehicles with this axle type were selected to reflect real-world loading conditions accurately. The wheelbases for 1.22-axle trucks range from 3.33 m to 6.69 m, depending on the vehicle brand in Türkiye; the shortest wheelbase, 3.3 m, was chosen to simulate a critical loading scenario.

Tire pressure for heavy vehicles generally varies from 500 to 1000 kPa worldwide, with 700 to 800 kPa recommended for pavement design (Moffatt 2017). Korkiala-Tanttu (2009) conducted extensive laboratory and ac-

celerated road tests, finding that the tire contact areas measured 250 mm by 225 mm for single tires and 225 mm by 200 mm for dual tires. In this study, a tire pressure of 700 kPa was applied, with contact areas of 250 mm by 225 mm for the front wheels and 225 mm by 200 mm for the rear wheels. A sample loading model for a pavement section with a 4.5-meter transverse joint spacing is illustrated in Fig. 2.

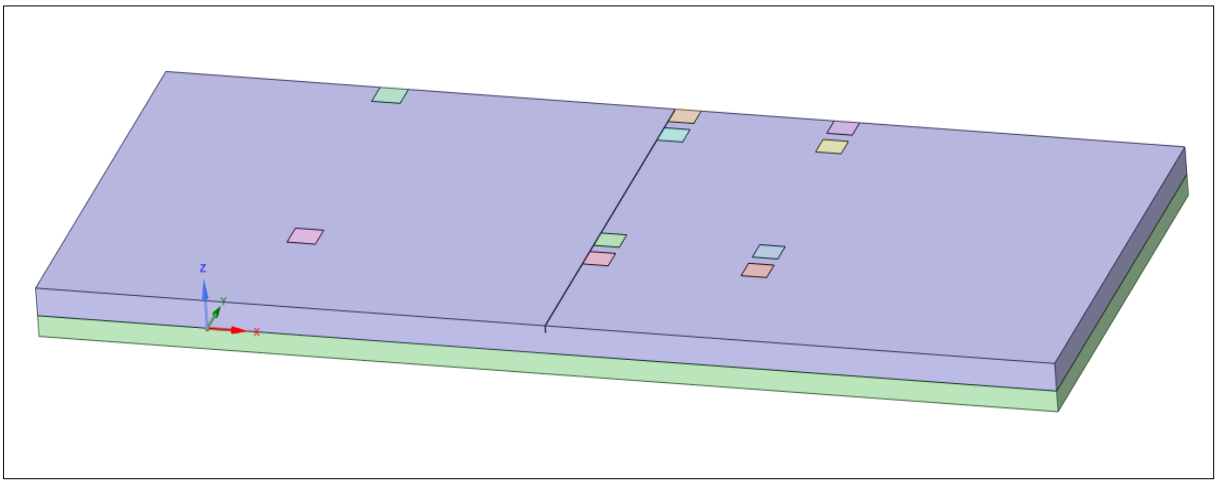

Fig. 2. Loading model of the pavement section with a 4.5-meter transverse joint spacing.

The finite element model consisted of a glass fiber-reinforced concrete pavement layer and a base layer arranged from top to bottom. The contact surface between the concrete pavement and the base layer was modeled as bonded. The base layer bottom was constrained in all directions, and the subgrade was excluded to improve the displacement analysis. Symmetry conditions were applied to the left side of the model, and the end faces along the y-axis were constrained in the x-axis to model the transverse joints. The right side of the model was not subjected to any constraints.

The element type SOLID185 was chosen for the base layer to represent the granular material. The modulus of elasticity was set at 100 MPa, 200 MPa, and 300 MPa, based on the AASHTO recommended range of 103 to 310 MPa. Poisson's ratio was set to 0.3. The base layer thickness was taken as 150 mm, the minimum thickness recommended by AASHTO.

ACPA (1992) and ACI 302.1R-11 (2011) recommend that joint spacing should be between 24 and 30 times the pavement thickness. Accordingly, the spacings for pavement thicknesses of 100 mm, 150 mm, and 200 mm were adjusted to 300 cm, 450 cm, and 600 cm, respectively, with the recommended upper limit. KGM (2016) recommends a joint width of 4.8 mm ± 1.5 mm and a minimum joint depth of one-fourth the concrete thickness. In this study, the joint width was considered to be 6 mm, and the depth was taken as one-fourth of the slab thickness.

2.2. Taguchi method

Finite element analyses were carried out using the Taguchi Method, which employs orthogonal arrays to minimize the number of experiments needed while maintaining the reliable confidence intervals (Mohammed and Najim 2020). In this approach, the S/N (Signal-to-Noise) ratio serves as a performance metric, where the signal represents the desired effect, and the noise reflects factors that adversely affect. Taguchi method addresses complex optimization problems through three solution targets: maximizing, minimizing, and achieving nominal values (Sünbül and Tortum 2024). Overall, this optimization process offers an effective and systematic approach, ensuring the production of high-performance, quality-enhanced products (Çolak et al. 2023).

The four parameters and their three levels, used for finite element analyses and optimization, are presented in Table 3. An L9 orthogonal array was selected for the experimental plan, with a 95% confidence interval applied; the details are provided in Table 4.

Table 3. Parameters and levels used in finite element analyses.

Parameters	Levels		
	1	2	3
Thickness (mm)	100	150	200
Glass fiber (%)	0.00	0.50	1.00
Modulus of elasticity of base layer (MPa)	100	200	300
Transverse joint space (mm)	300	450	600

Table 4. Experimental plan for finite element analysis.

Experiment No.	Thickness (mm)	Glass fiber (%)	Modulus of elasticity of base layer (MPa)	Joint space (mm)
1	100	0.00	100.00	300
2	100	0.50	200.00	450
3	100	1.00	300.00	600
4	150	0.00	200.00	600
5	150	0.50	300.00	300
6	150	1.00	100.00	450
7	200	0.00	300.00	450
8	200	0.50	100.00	600
9	200	1.00	200.00	300

3. Results and Discussion

3.1. Validation of the established FEM models

To validate the established models using compression and flexural test data on a concrete slab, Experiment 5 was selected. The model analysis results of the compression test for equivalent stress and equivalent total strain are shown in Fig. 3, with maximum equivalent stress and maximum equivalent total strain values of 36.87 MPa and 0.0022703 mm/mm, respectively.

The model analysis results of the flexural test for maximum principal stress and equivalent total strain are shown in Fig. 4, with maximum principal stress and maximum equivalent total strain values of 4.6791 MPa and 0.001834 mm/mm, respectively.

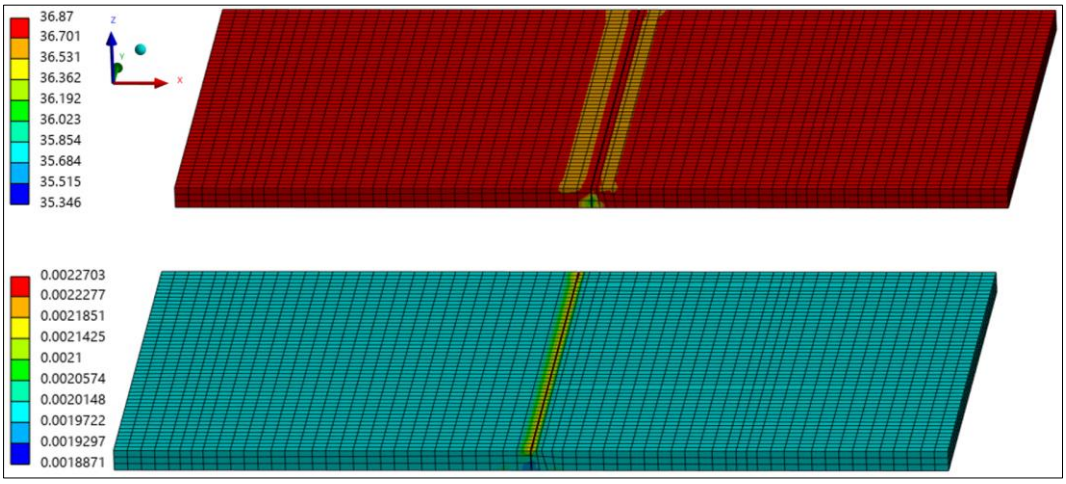

Fig. 3. Validation of compression test on a concrete slab for Experiment 5: Equivalent stress and equivalent total strain.

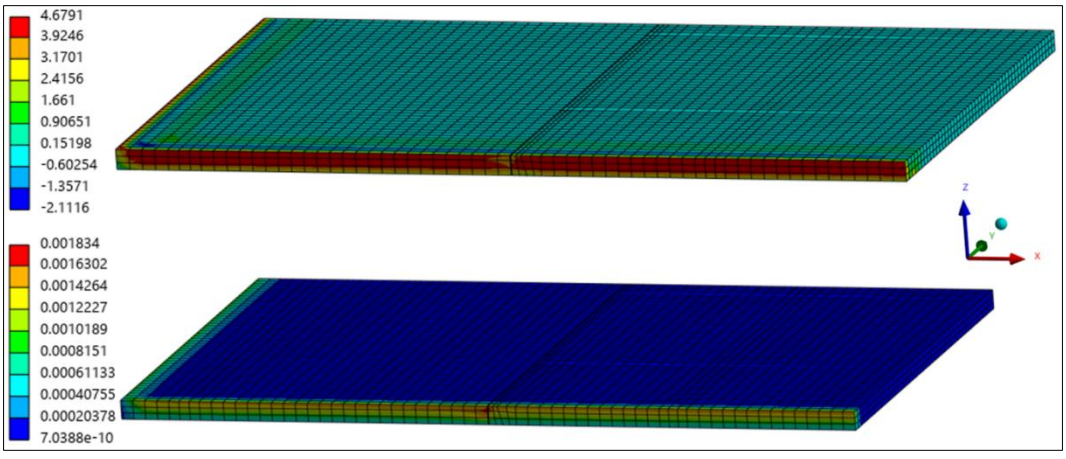

Fig. 4. Validation of flexural test on a concrete slab for Experiment 5: Maximum principal stress and equivalent total strain.

Fig. 5 presents the comparison between finite element analysis results and test data for compression and flexural tests. A reasonable agreement was observed, confirming the suitability of the selected constitutive iron cast model for simulating the real behavior of glass fiber-reinforced concrete.

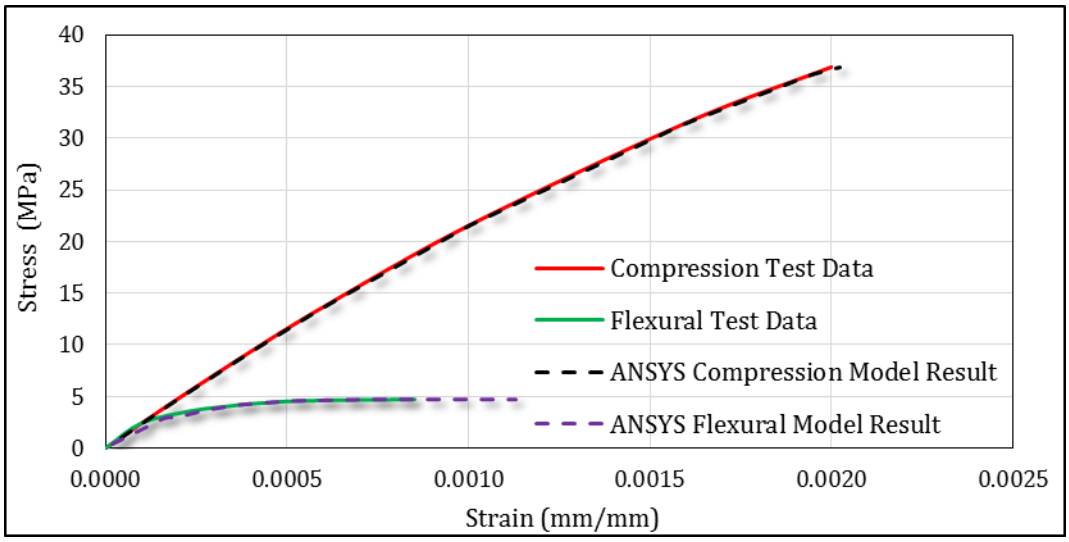

Fig. 5. Comparison of finite element results with compression and flexural tests.

3.2. Maximum principal stress analysis results

Maximum principal stress results used to evaluate the flexural stress arising at the bottom of the glass fiber-reinforced concrete layer are presented in Fig. 6.

As shown in Table 5, an ANOVA (Analysis of Variance) test was conducted to determine whether the S/N values of finite element results are statistically significant and to enable estimations with a 95% confidence interval. This study's error degree of freedom is zero, as all four parameters have three levels. To increase the error degree of freedom and enable estimations at a %95 confidence level, the transverse joint spacing parameter, with the smallest contribution at 0.28%, was pooled. The model demonstrated a high level of accuracy, with an R^2 of 0.9972 and a predicted R^2 of 0.9434, both in close agreement with the adjusted R^2 of 0.9888 (difference < 0.2). Additionally, the adequate precision, an indicator of signal-to-noise ratio, was 30.97, well above the threshold of 4, confirming the model's suitability for navigating the design space.

At a 95% confidence level, the F-values for the remaining parameters (concrete thickness, glass fiber ratio, and modulus of elasticity of the base layer) were higher than the F-table value of 19 for (2;2). Additionally, the model is statistically significant, as all unpooled parameters have p-values below 0.05.

The S/N contributions of all parameters are given in Table 6. The optimum levels were identified as A3, B3, C3, and D3. As shown in the experiment plan in Table 4, no experiment includes the optimum levels.

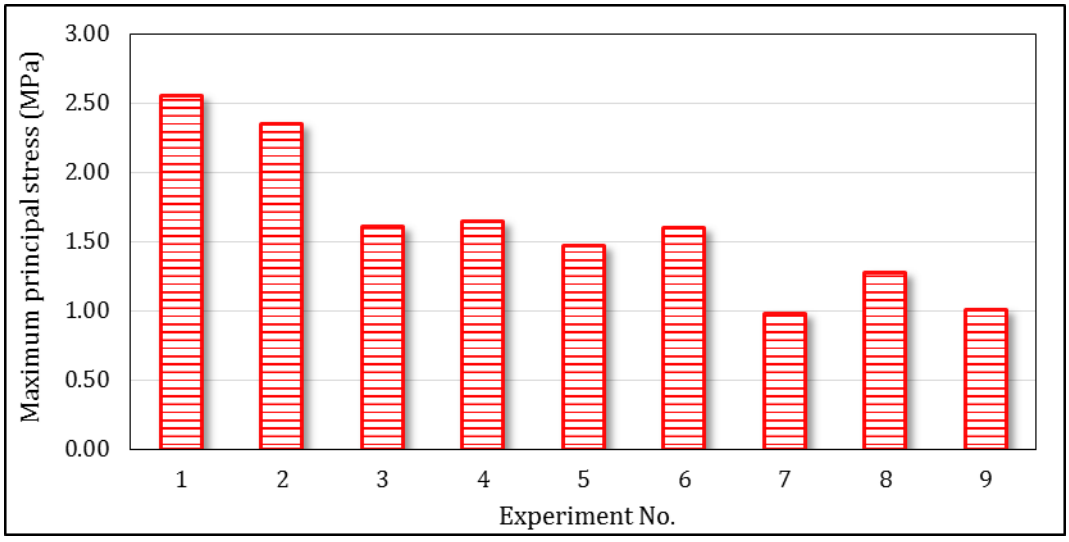

Fig. 6. Maximum principal stress results according to the experimental plan.

Table 5. Taguchi ANOVA table for maximum principal stress results.

Parameters	df	Sums of squares	Variance	F-value	Contribution (%)	p-value
Thickness (mm)	2	52.41	26.20	287.65	80.43	0.003
Glass fiber (%)	2	4.11	2.05	22.55	6.31	0.042
Modulus of elasticity of base layer (MPa)	2	8.46	4.23	46.45	12.99	0.021
Joint space (mm)			Pooled			
Error	2	0.18	0.09		0.28	
Total	8	65.16			100	

Table 6. S/N contributions of all parameters.

Parameters	Optimum levels	S/N contribution
Thickness (mm)	3	3.052
Glass fiber (%)	3	0.949
Modulus of elasticity of base layer (MPa)	3	1.284
Joint space (mm)	3	0.000
The sum of contributions (S/N)		5.285
Average performance statistics (S/N)		-3.716
Optimum predicted result (S/N) / (MPa)		1.569 / 0.835
Validation result (S/N) / (MPa)		0.141 / 0.98393
Confidence interval (α=95%) (S/N)		- 0.162 - 3.301

A validation finite element model was created using the optimum levels: 200 mm concrete thickness, 1% glass fiber ratio, 300 MPa modulus of elasticity of the base layer, and 600 mm joint spacing. The maximum principal stress in the validation finite element model was observed to be 0.98393 MPa, located at the bottom of the concrete layer at the transverse joint, as shown in Fig. 7. This value falls within the range of 0.684 to 1.018 MPa, indicating that the result is accurate within a 95% confidence interval.

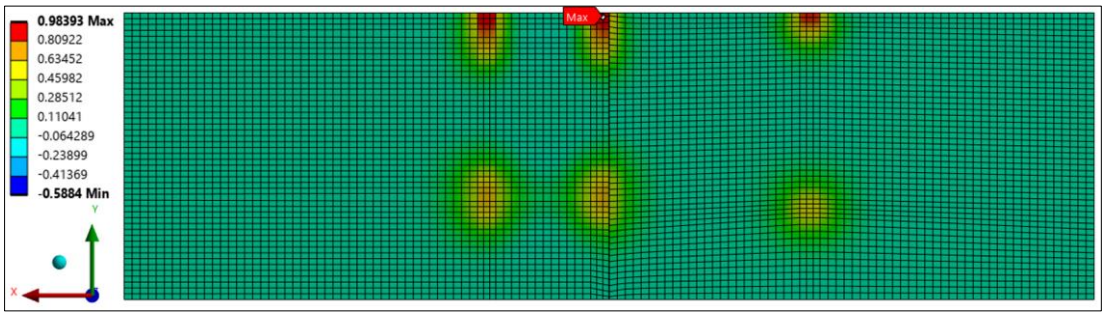

Fig. 7. Maximum principal stress at the bottom of the concrete slab for validation model.

Performance statistics for minimizing maximum principal stress values are shown in Fig. 8. The signal-to-noise (S/N) contribution of the concrete slab thickness was found to be the most effective parameter in minimizing flexural stress at the bottom of the concrete layer, with a value of 3.052. This was followed by the modulus of elasticity of the base layer, glass fiber ratio, and joint spacing, with respective values of 1.284, 0.949, and 0.194.

As the concrete thickness increased, the maximum principal stress at the bottom of the slab decreased significantly, consistent with previous studies (Sultana 2010; Baş et al. 2022). This is attributed to the higher load transfer efficiency of the thicker plates, particularly at the joints (Sii 2015). The 0.5% glass fiber ratio had a similar effect on maximum principal stress as plain concrete (showing no significant impact), while the 1.0% glass fiber ratio reduced the maximum principal stress. The theoretical critical fiber volume, the amount of fiber needed to significantly impact the concrete's strength, is between 1% and 3% (Bentur and Mindess 2006). Since the 0.5% fiber ratio was below this threshold, it had a similar effect to the plain concrete. The 1.0% ratio's effectiveness is attributed to the strong bond between the

fibers and the concrete matrix, causing the fibers to fracture before debonding (Roesler et al. 2019). The maximum principal stress decreased as the modulus of elasticity of the base layer increased, aligning with previous studies conducted on concrete slabs (Wu et al. 1993; Kim 2017). The transverse joint spacing had the least effect on maximum principal stress; however, it is important to note that increasing the transverse joint spacing may lead to more cracking in the concrete slab (Shoukry et al. 2007; Roesler et al. 2019).

3.3. Total deformation analysis results

Total deformation results obtained from the finite element models on the glass fiber-reinforced concrete layer are presented in Fig. 9.

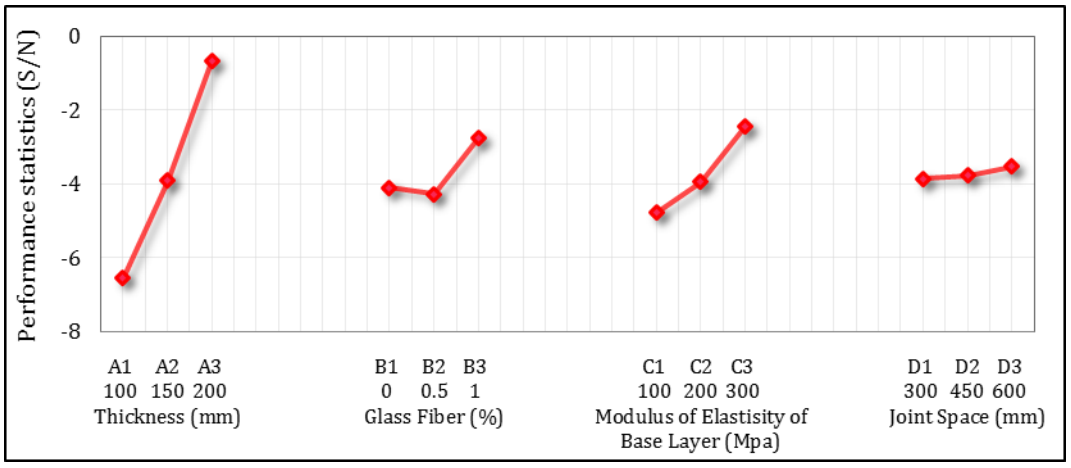

Fig. 8. Performance statistics minimizing maximum principal stress for all levels.

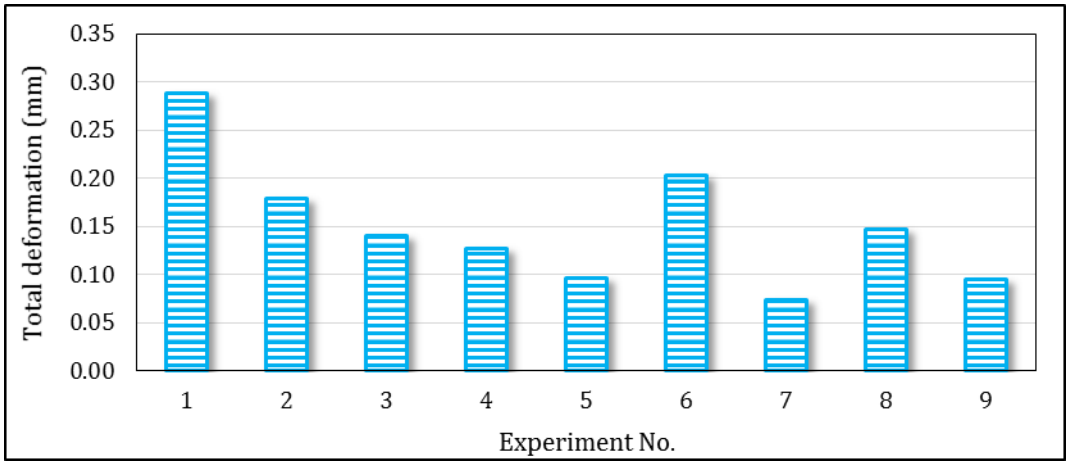

Fig. 9. Total deformation results according to the experimental plan.

As shown in Table 7, the Taguchi ANOVA table for total deformation results demonstrates a perfect model fit. With an R^2 of 0.9998, the model achieves error-free prediction accuracy by accounting for all variability in the total deformation results. Furthermore, the predicted R^2 of 0.9996 and adjusted R^2 of 0.9997 highlight the model's robustness and reliability, confirming its predictive power without the risk of overfitting.

Table 7. Taguchi ANOVA table for total deformation results.

Parameters	df	Sums of squares	Variance	F-value	Contribution (%)	p-value
Thickness (mm)	2	48.468	24.234	20,812	44.16	0.00005
Glass fiber (%)	2	0.056	0.028	24.096	0.05	0.03985
Modulus of elasticity of base layer (MPa)	2	61.242	30.621	26,297	55.79	0.00004
Joint space (mm)			Pooled			
Error	2	0.002	0.001			
Total	8	109.768			100	

The performance statistics for the total deformation results are shown in Fig. 10. The optimal levels for minimizing total deformation in the concrete layer were identified as A3, B2, C3, and D1. The base layer modulus of elasticity made the highest contribution to reducing total deformation, with a value of 55.79, followed by the concrete layer thickness at 44.16. Glass fiber had a minor contribution of 0.05, and transverse joint spacing, contributing only 0.002, was therefore pooled. As both the base layer modulus of elasticity and concrete thickness increased, total deformation decreased. The concrete layer became stiffer with the increased thickness, and this situation led to less deformation under the vehicle loads since it distributed the vehicle load more effectively through the pavement. The increase in the elasticity modulus of the base layer led to lower deformation, as it measures the layer's rigidity. The effect of the glass fiber ratio on deformation was minor compared to the thickness and the base layer's modulus of elasticity. Although the increase in elasticity modulus and flexural strength slightly improved the concrete material's stiffness, the impact was limited because the vehicle loading with a 1.22 axle type did not generate stresses at the edge and transverse joint high enough to exceed the tensile yield strength, keeping the material within the elastic region and preventing it from entering the plastic region. Transverse joint spacing had a minimal effect on deformation; however, it is important to note that shorter transverse joint spacings are necessary for stiffer base layers to reduce the risk of transverse cracking (Huang 2004).

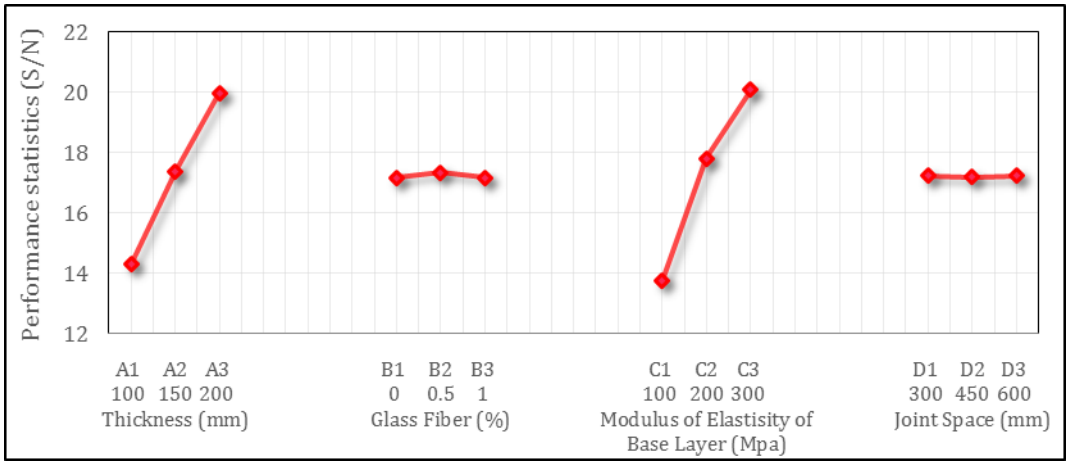

Fig. 10. Performance statistics minimizing total deformation for all levels.

The maximum total deformation observed in the finite element model for validating maximum principal stress optimization at levels A3, B3, C3, and D3 was 0.072384 mm, located at the transverse joint, as shown in Fig. 11. This value falls within the range of 0.0709894 to 0.0742625, confirming model accuracy within a 95% confidence interval.

3.4. Equivalent total strain analysis results

Equivalent total strain results obtained from the finite element models on the glass fiber-reinforced concrete layer and corresponding S/N values are presented in Table 8.

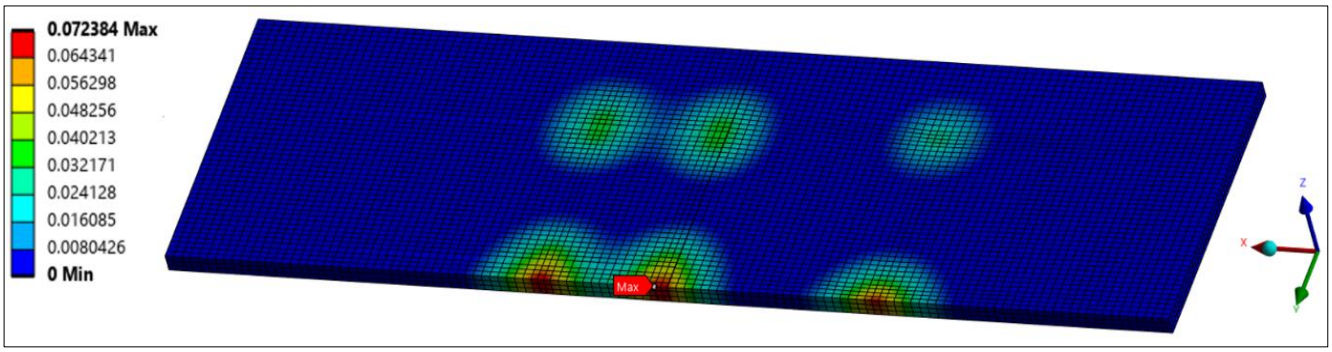

Fig. 11. Total deformation result at levels A3, B3, C3, and D3.

The ANOVA table for minimizing the maximum equivalent total strain results is given in Table 9. The close alignment between R^2 (0.9997), adjusted R^2 (0.9996) and predicted R^2 (0.9993) confirms that the model is well-fitted and robust without overfitting and bias. The high predicted R^2 value, close to 1.00, validates the model's estimation capability. Optimum levels that minimize the equivalent total strains were found as A3, B2, C3, and D3.

Table 8. Equivalent total strain results and corresponding S/N values.

Experiment No.	Equivalent total strain (mm/mm)	S/N
1	0.00188930	54.47
2	0.00112380	58.99
3	0.00086532	61.26
4	0.00081253	61.80
5	0.00060235	64.40
6	0.00131750	57.60
7	0.00046139	66.72
8	0.00096555	60.30
9	0.00060722	64.33

Table 9. Taguchi ANOVA table for equivalent total strain results.

Parameters	df	Sums of squares	Variance	F-value	Contribution (%)	p-value
Thickness (mm)	2	46.279	23.140	11,364	40.36%	0.00009
Glass fiber (%)	2	0.086	0.043	21.166	0.08%	0.04511
Modulus of elasticity of base layer (MPa)	2	68.301	34.151	16,771	59.56%	0.00006
Joint space (mm)			Pooled			
Error	2	0.004	0.002			
Total	8	114.671			100	

The modulus of elasticity of the base layer and concrete thickness had the greatest impact in minimizing the equivalent total strain, with values of 59.56 and 40.36, respectively. In contrast, the glass fiber ratio and joint spacing parameters had minimal effects, with values of 0.075 and 0.004. The equivalent total strain decreased as both the modulus of elasticity of the base layer and the thickness of the concrete layer increased.

The finite element model for validating maximum principal stress optimization at levels A3, B3, C3, and D3 showed a maximum equivalent total strain of 0.00045942 mm at the transverse joint, as illustrated in Fig. 12. This value lies within the range of 0.000444698 to 0.000472011, verifying model accuracy within a 95% confidence interval.

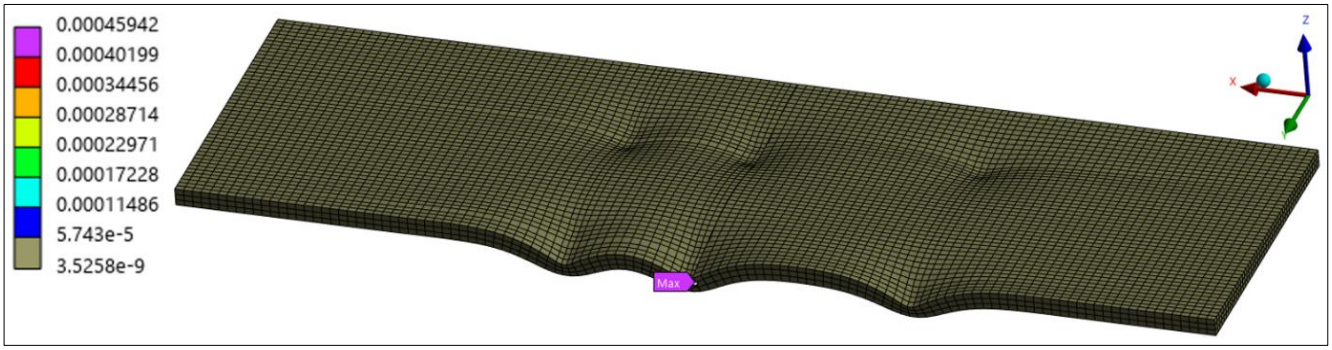

Fig. 12. Equivalent total strain result at levels A3, B3, C3, and D3 (0.5x Auto scaled).

The high predicted R^2 value for all three models validates the robustness of the model's predictive ability. The transverse joint spacing parameter was pooled for all three models, and predictions were made without this parameter, considering all remaining factors across all levels at a 95% confidence level, as summarized in Table 10.

4. Conclusions

This study evaluated the addition of glass fibers at 0%, 0.5%, and 1% to enhance the flexural strength of concrete pavements, examining the effects on maximum principal stress, total deformation, and equivalent total strain. The concrete pavements had thick-

nesses of 100, 150, and 200 mm, with base layer elastic moduli of 100, 200, and 300 MPa, and transverse joint spacings of 300, 450, and 600 mm. The findings are summarized below:

Table 10. Taguchi predictions for all parameters except transverse joint spacing.

Levels	Maximum principal stress (MPa)	Total deformation (mm)	Equivalent total strain (mm/mm)
A1-B1-C1	2.513	0.288	0.00188318
A1-B1-C2	2.283	0.181	0.00115498
A1-B1-C3	1.919	0.139	0.00087427
A1-B2-C1	2.568	0.283	0.00183341
A1-B2-C2	2.333	0.178	0.00112445
A1-B2-C3	1.961	0.137	0.00085117
A1-B3-C1	2.156	0.289	0.00186887
A1-B3-C2	1.959	0.181	0.00114620
A1-B3-C3	1.646	0.140	0.00086763
A2-B1-C1	1.853	0.202	0.00132836
A2-B1-C2	1.683	0.127	0.00081470
A2-B1-C3	1.415	0.098	0.00061670
A2-B2-C1	1.894	0.198	0.00129325
A2-B2-C2	1.720	0.125	0.00079317
A2-B2-C3	1.446	0.096	0.00060040
A2-B3-C1	1.590	0.202	0.00131827
A2-B3-C2	1.444	0.127	0.00080851
A2-B3-C3	1.214	0.098	0.00061201
A3-B1-C1	1.274	0.150	0.00099441
A3-B1-C2	1.157	0.094	0.00060988
A3-B1-C3	0.973	0.073	0.00046166
A3-B2-C1	1.302	0.147	0.00096813
A3-B2-C2	1.183	0.092	0.00059377
A3-B2-C3	0.994	0.071	0.00044946
A3-B3-C1	1.093	0.150	0.00098685
A3-B3-C2	0.993	0.094	0.00060525
A3-B3-C3	0.835	0.073	0.00045815

- The concrete thickness and the base layer modulus of elasticity were the most influential factors in minimizing stress, deformation, and strain, with greater thickness and stiffness resulting in improved pavement performance. The glass fiber addition had a more notable impact on maximum principal stress, especially at the 1% ratio, but had a minimal effect on total deformation and strain. Transverse joint spacing had the least effect, although shorter spacings are still recommended to reduce the risk of transverse cracking in stiffer base layers.
- Across all levels of glass fiber ratio and base layer elasticity modulus, concrete thicknesses of 100 mm and 150 mm produced maximum principal stresses approximately 1.97 and 1.45 times higher, respectively, than the thickness of 200 mm. These thicknesses also led to deformations and strains approximately 1.91 and 1.35 times higher, respectively, compared to the 200 mm thickness.
- Similarly, across all levels of glass fiber ratio and concrete thickness, base layer elasticity moduli of 100 MPa and 200 MPa generated maximum principal stresses about 1.31 and 1.19 times higher, respectively, than a modulus of 300 MPa. These moduli also resulted in deformations and strains approximately 2.11 and 1.31 times greater than those observed with a modulus of 300 MPa.
- Lastly, across all levels of concrete thickness and base layer elasticity modulus, glass fiber ratios of 0% and 0.5% produced maximum principal stresses approximately 1.18 times higher than a ratio of 1%. No effect of glass fiber ratio on deformation and strain was observed.

Acknowledgements
None declared.

Funding
The author received no financial support for the research, authorship, and/or publication of this manuscript.

Conflict of Interest
The author declared no potential conflicts of interest with respect to the research, authorship, and/or publication of this manuscript.

Data Availability
The datasets created and/or analyzed during the current study are not publicly available, but are available from the corresponding author upon reasonable request.

REFERENCES

Abdulridha MA, Salman MM, Banyhussan QS (2021). Effect polypropylene of fiber on drying shrinkage cracking of concrete pavement using response surface methodology. *Journal of Engineering Sustainable Development,* 25(3), 10-21.

ACI 302.1R-11 (2011). Guide to concrete floor and slab construction. American Concrete Institute, Farmington Hills, MI.

ACPA (1992). Design and construction of joints for concrete streets. American Concrete Pavement Association, Skokie, IL.

Afroz M, Venkatesan S, Patnaikuni I (2019). Effects of hybrid fibers on the development of high volume fly ash cement composite. *Construction and Building Materials,* 215, 984-997.

Ağar E, Sütaş İ, Öztaş G (1998). Beton Yollar: Rijit Yol Üstyapıları; Malzeme-Tasarım-Üretim-Yapım-Bakım Teknikler. İstanbul Technical University, İstanbul. (in Turkish)

Akram H, Hozayen HA, Abdelfatah A, Khodary F (2024). Fiber showdown: A comparative analysis of glass vs. polypropylene fibers in hot-mix asphalt fracture resistance. *Buildings,* 14(9), 2732.

Ali B, Qureshi LA (2019). Influence of glass fibers on mechanical and durability performance of concrete with recycled aggregates. *Construction and Building Materials,* 228, 116783.

Ali B, Qureshi LA, Khan SU (2020). Flexural behavior of glass fiber-reinforced recycled aggregate concrete and its impact on the cost and carbon footprint of concrete pavement. *Construction Building Materials,* 262, 120820.

Araz NG, Aksoy A, Aslan MT and İskender E (2023). Asfalt kaplamalarda bitüm oranına bağlı olarak sıkıştırma sıcaklığının etkisinin Marshall Deneyi parametreleri ile incelenmesi. *Recep Tayyip Erdogan University Journal of Science and Engineering,* 4(1), 39-50. (in Turkish)

ASTM-C39 (2015). Standard test method for compressive strength of cylindrical concrete specimens. ASTM International, West Conshohocken, PA.

ASTM-C78 (2018). Standard test method for flexural strength of concrete (using simple beam with third-point loading). ASTM International, West Conshohocken, PA.

Baş Fİ, Bayrak OÜ, Bayata HF (2022). A Practical design guide for unbonded jointed plain concrete roads over deteriorated HMA roads: Realistic traffic loading. *Coatings,* 12(12), 1817.

Bentur A, Mindess S. (2006). Fibre Reinforced Cementitious Composites. CRC Press, Boca Raton, FL.

Bhogone M, Subramaniam KV (2022). Improvement in early-age cracking performance of concrete with hybrid steel-macropolypropylene fiber blends. *Materials Today: Proceedings,* 65, 1589-1593.

Cheung Y, Zinkiewicz O (1965). Plates and tanks on elastic foundations–an application of finite element method. *International Journal of Solids Structures,* 1(4), 451-461.

Çelik M (2014). Karadeniz Bölgesi Köy Yolları için Rijit ve Esnek Kaplamanın Mekanistik ve Maliyet Açısından Karşılaştırılması. *M.Sc. thesis*, Karadeniz Technical University, Trabzon. (in Turkish)

Çelik Z, Turan E, Oltulu M, Öner G (2024). Reinforcement of concrete beams using waste carbon-nanoclay-fiberglass laminate pieces. *Challenge Journal of Concrete Research Letters*, 15(1), 1-6.

Çolak MA, Zorlu E, Çodur MY, Baş Fİ, Yalçın Ö, Kuşkapan E (2023). Investigation of physical and chemical properties of bitumen modified with waste vegetable oil and waste agricultural ash for use in flexible pavements. *Coatings,* 13(11), 1866.

Eryılmaz Yıldırım M, Aybar K, Canbaz M (2024). Size effect on compressive behavior of GFRP bars. *Challenge Journal of Structural Mechanics*, 10(1), 14-20.

Gultekin A (2023). Effect of hemp and basalt fiber on fracture energy of cement-based composites: a comparative study. *Challenge Journal of Concrete Research Letters*, 14(4), 107-117.

Huang YH (2004). Pavement Analysis and Design (vol. 2). Pearson Prentice Hall, Upper Saddle River, NJ.

Hussain I, Ali B, Akhtar T, Jameel MS, Raza SS (2020). Comparison of mechanical properties of concrete and design thickness of pavement with different types of fiber-reinforcements (steel, glass, and polypropylene). *Case Studies in Construction Materials,* 13, e00429.

Jagannadha RK, Ahmed KT (2009). Suitability of glass fibers in high strength recycled aggregate concrete-An experimental investigation. *Asian Journal of Civil Engineering (Building and Housing),* 10(6), 681-689.

Jawdhari A, Fam A (2020). Thermal-structural analysis and thermal bowing of double Wythe UHPC insulated walls. *Energy Buildings,* 223, 110012.

Karahan O, Atiş CD (2011). The durability properties of polypropylene fiber reinforced fly ash concrete. *Materials Design,* 32(2), 1044-1049.

KGM (2016). Beton Yol Kaplamaları Teknik Şartnamesi. General Directorate of Highways, Ankara. (in Turkish)

KGM (2023). Trafik ve ulaşım bilgileri, otoyollar ve devlet yollarinin trafik dilimlerine göre yillik ortalama günlük trafik değerleri ve ulaşim bilgileri. General Directorate of Highways, Ankara. (in Turkish)

KGM (2024). Yol Ağı Bilgileri. Karayolları Genel Müdürlüğü. https://www.kgm.gov.tr/Sayfalar/KGM/SiteTr/Kurumsal/YolAgi.aspx [accessed 20-08-2024] (in Turkish)

Kim K (2017). Enhanced Finite Element Analysis Tools and Instrumentation Method to Evaluate the Structural Behavior of Non-Conventional Concrete Pavements. *Ph.D. thesis*, University of Florida, Gainesville, FL.

Kizilkanat AB, Kabay N, Akyüncü V, Chowdhury S, Akça AH (2015). Mechanical properties and fracture behavior of basalt and glass fiber reinforced concrete: An experimental study. *Construction and Building Materials, 100*, 218-224.

Korkiala-Tanttu L (2009). Calculation Method for Permanent Deformation of Unbound Pavement Materials. VTT Publications, Helsinki.

Kosmatka SH, Kerkhoff B, Panarese WC (2003). Design and Control of Concrete Mixtures. Engineering Bulletin 001, Portland Cement Association, Skokie, Illinois.

Kumara W, Tia M, Wu C-L, Choubane B (2003). Evaluation of applicability of ultra-thin whitetopping (UTW) in Florida*. 2003 Annual Transportation Research Board Meeting*.

Lau CK, Chegenizadeh A, Htut TN, Nikraz H (2020). Performance of the steel fibre reinforced rigid concrete pavement in fatigue. *Buildings,* 10(10), 186.

Moaveni S (2011). Finite element analysis theory and application with ANSYS, 3/e. Pearson Education, India.

Moffatt M (2017). Guide to Pavement Technology Part 2: Pavement Structural Design. Austroads Ltd., Sydney, Australia.

Mohammed SI, Najim KB (2020). Mechanical strength, flexural behavior and fracture energy of recycled concrete aggregate self-compacting concrete. *Structures,* 23, 34-43.

Mola E, Bayrak OÜ, Baş Fİ, Bayata HF (2024). Investigating the usability of kevlar and steel fibers as a hybrid in concrete pavements. *Sigma Journal of Engineering Natural Sciences,* 42(2), 344-355.

Nazki MA, Chopra T, Chandrappa AK (2020). Rheological properties and thermal conductivity of bitumen binders modified with graphene. *Construction and Building Materials,* 238, 117693.

Nguyen Dinh N (2016). Precast ultra-thin whitetopping (PUTW) in Singapore and its application for electrified roadways. *Ph.D. thesis*, Technische Universität, München,

Noorvand H, Arce GA, Hassan MM (2022). Evaluation of the effects of engineered cementitious composites (ECC) plasticity on concrete pavement performance. *International Journal of Pavement Engineering,* 23(13), 4474-4486.

Ntimugura F, Vinai R, Harper A, Walker P (2020). Mechanical, thermal, hygroscopic and acoustic properties of bio-aggregates–lime and alkali-activated insulating composite materials: a review of current status and prospects for miscanthus as an innovative resource in the South West of England. *Sustainable Materials Technologies,* 26, e00211.

Roesler J, Bordelon A, Brand AS, Amirkhanian A (2019). Fiber-reinforced concrete for pavement overlays: Technical overview. In-Trans Project, 15-532.

Roesler JR, Lange DA, Altoubat SA, Rieder K-A, Ulreich GR (2004). Fracture of plain and fiber-reinforced concrete slabs under monotonic loading. *Journal of materials in Civil Engineering,* 16(5), 452-460.

SAS (2024). ANSYS Engineering Simulation Student Software. SAS IP Inc.

Sharbatdar MK, Rahmati F (2022). Experimental evaluation of multifunctional effects of fibers on mechanical and performance properties of Roller-compacted concrete pavements (RCCP). *Construction and Building Materials,* 316, 125890.

Shoukry SN, Fahmy M, Prucz J, William G (2007). Validation of 3DFE analysis of rigid pavement dynamic response to moving traffic and nonlinear temperature gradient effects. *International Journal of Geomechanics,* 7(1), 16-24.

Sii HB (2015). Three-Dimensional Finite Element Analysis of Concrete Pavement on Weak Foundation. *Ph.D. thesis,* Griffith University, Queensland, Australia.

Sultana S (2010). Extending Asphalt Pavement Life with Thin Whitetopping. *Ph.D. thesis,* Kansas State University, Manhattan, KS.

Sünbül Ş, Tortum A (2024). Investigation of the use of nano powder on roller compressible fibrous concrete roads. *Case Studies in Construction Materials,* 21, e03572.

Şengel H, Kınık K, Erol H, Canbaz M (2022). Effect of waste steel tire wired concrete on the mechanical behavior under impact loading. *Challenge Journal of Structural Mechanics*, 8(4), 150-158.

Tunçel M, Bayrak OÜ, Baş Fİ, Bayata HF (2020). Atık kevların beton yol kaplamalarında kullanılabilirliğinin araştırılması. *Avrupa Bilim ve Teknoloji Dergisi,* 19, 668-678. (in Turkish)

Wu C, Tia M, Larsen T (1993). Analysis of structural response of concrete pavements under critical thermal-loading conditions. *5th International Conference on Concrete Pavement Design and Rehabilitation,* Purdue University, Lafayette, Ind., 1, 317–340. USA.

Zain MFM, Mahmud H, Ilham A, Faizal M (2002). Prediction of splitting tensile strength of high-performance concrete. *Cement Concrete Research,* 32(8), 1251-1258.

Zhang P, Li Q-f (2013). Effect of polypropylene fiber on durability of concrete composite containing fly ash and silica fume. *Composites Part B: Engineering,* 45(1), 1587-1594.